Characteristic Analysis of Wind Turbine Gearbox Considering Non-Torque Loading

Young-Jun Park
Senior Researcher
e-mail: yjpark77@kimm.re.kr

Geun-Ho Lee
Principal Researcher
e-mail: ghlee762@kimm.re.kr

Jin-Seop Song
Senior Researcher
e-mail: jssong@kimm.re.kr

Yong-Yun Nam
Principal Researcher
e-mail: yynam@kimm.re.kr

Department of System Reliability,
Korea Institute of Machinery & Materials,
Daejeon 305-343, Republic of Korea

In the design of wind turbine gearboxes, the most important objective is to improve the durability to guarantee a service life of more than 20 years. This work investigates how external loads caused by wind fluctuation influence both the load distribution over the gear tooth flank and the planet load sharing. A whole system model is developed to analyze a wind turbine gearbox (WTG) that consists of planetary gearsets. Two models for different design loads are employed to quantify how external loads acting on the input shaft of the WTG affect the load distribution of the gears and the load sharing among the planets under quasi-static conditions. One model considers only the torque for the design load, whereas the other model also considers non-torque loads. For two models, the results for the gear mesh misalignment, contact pattern, load distribution, and load sharing are different, and this leads to different gear safety factors. Therefore, the results indicate that it is appropriate to consider the non-torque loads in addition to the torque as the design load for a WTG, and that this is very important to accurately determine the design load that guarantee the service life of a WTG. [DOI: 10.1115/1.4023590]

Keywords: wind turbine gearbox (WTG), non-torque loads, gear mesh misalignment, load distribution, load sharing

1 Introduction

The wind power generation industry has recently received much attention as a source of alternative energy. The most critical issues in this industry are the performance and service life of the wind turbine system used to convert wind energy into electrical energy. This wind turbine system is composed of several blades, a rotor, gearboxes, a generator, a tower, and control systems. The wind turbine gearbox (WTG) is well known as the component with the highest failure rate [1].

The WTG, which is located between the rotor blades and generator, converts the input power of the rotor blades and then transmits this power to the generator. The input shaft from the rotor blades has a low rotational speed of 12–30 rpm and high torque, while the output shaft to the generator has a high rotational speed of 1000–1800 rpm and low torque. Whenever the wind turbine system operates, any wind load fluctuation applies high dynamic forces and moments to the gears, bearings, and shafts that compose the WTG. This phenomenon has an adverse influence upon the strength and durability of the WTG, perhaps causing the initial failure and reducing the service life. The WTG is required to have a service life of more than 20 years [2]. Therefore, the most important concern for the WTG is to improve the durability to guarantee the service life, and it is keenly desired that a WTG design process for high durability be established.

Many studies have been performed on how numerous manufacturing and assembly errors related to the carrier and gears influence the load sharing among the planets. Bodas and Kahraman [3] used a two-dimensional deformable-body model of a planetary gearset to theoretically demonstrate that adding more planets makes the gear system more sensitive to manufacturing errors and assembly variations in the carrier and gears. They stated that a large number of manufacturing errors influence the planet load sharing characteristics. Singh [4] used a three-dimensional model of the same configuration to reach similar conclusions. His analysis indicated that the pinhole position errors were directionally sensitive, and the errors in the tangential direction had the most critical influence on planet load sharing. Kahraman and Vijayakar [5] used a two-dimensional deformable-body model of a planetary gearset to investigate the effect of a flexible internal gear on the quasi-static behavior of a planetary gearset. They concluded that a flexible internal gear improves the load sharing among the planets but is not as effective as the method of floating the sun gear. The models used in previous studies to investigate load sharing among the planets considered the torque to be the only external load. However, it is important to consider external loads aside from torque, as well as the nonlinear characteristics of the bearings, when the WTG is designed and analyzed.

In order to meet the service life of the WTG, the most critical design factors are the load distribution and load sharing among the gears. In the case of a PGS, the loads acting on gears should be distributed evenly over the gear tooth flank and shared equally by several planets to increase the gear life. This study investigates how the external loads caused by wind fluctuation influence both the load distribution over the gear tooth flank and the planet load sharing. A state-of-the-art nonlinear system model is developed to analyze the planetary gearset for the WTG. This model includes the nonlinear mesh stiffness of the gears and the nonlinear stiffness of the bearings, as well as the flexibilities of the housing, planet carriers, and ring gears. Two models with different design load cases are employed to quantify how the external loads acting on the input shaft of the WTG affect the load distribution of the gears and the load sharing among the planets under the quasi-static conditions. The first model considers only the torque for the design load; namely, the design method for general industrial gearboxes is used. The second model considers non-torque loads as well as the torque for the design loads. A design method to guarantee the service life of the WTG is also presented.

2 Modeling of Wind Turbine Gearbox

2.1 Structure of Wind Turbine Gearbox. The WTG used in this study is a typical gearbox for a 2 MW wind turbine system and is composed of a low-speed planetary gearset (LS PGS), high-speed planetary gearset (HS PGS), and parallel helical gearset, as shown in Fig. 1. The load condition for the two PGSs is as follows: the input load is on the planet carrier, the ring gear is fixed, and the output load is from the sun gear.

Contributed by the Power Transmission and Gearing Committee of ASME for publication in the JOURNAL OF MECHANICAL DESIGN. Manuscript received July 20, 2012; final manuscript received January 10, 2013; published online March 22, 2013. Assoc. Editor: Qi Fan.

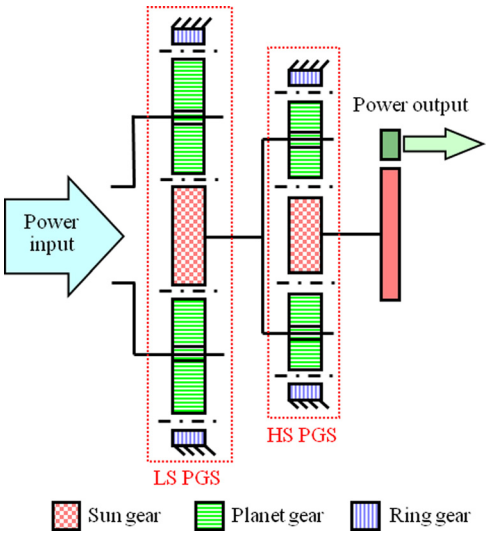

Fig. 1 Structure of 2 MW WTG in this study

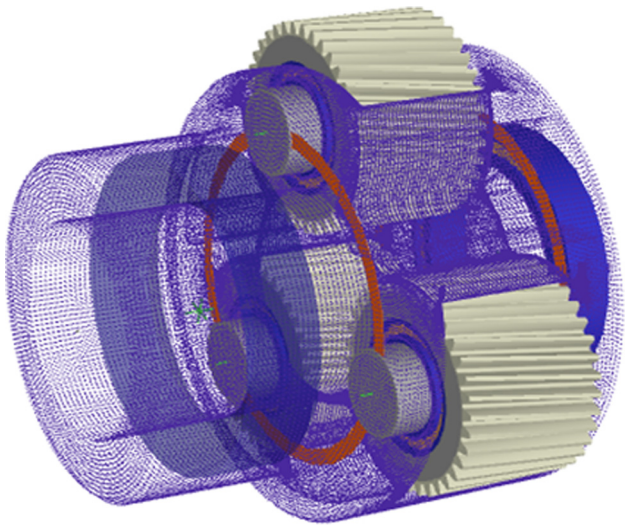

Fig. 2 Model of planetary gearset

2.2 Physical Model of Wind Turbine Gearbox. The entire 2 MW WTG is modeled in detail. The model is used to carry out a quasi-static analysis of a gearbox by linking the shafts, bearings, gears, planet carriers, and housing. Because a whole system model of the WTG is made by considering nonlinear components such as the bearing stiffness and gear mesh stiffness, the system deflections such as the gear mesh misalignment, bearing deformations, and deflections of the shafts, planet carriers, and housing can be analyzed simultaneously. The model can also predict the gear life and bearing life by using the system deflection results.

Within the system model, the spur and helical gears are defined using the stiffness under contact and described in terms of macro-geometric parameters such as the number of teeth, module, helix angle, pressure angle, center distance, and profile shift, as well as micro-geometric parameters such as the crowning and lead slope. The behavior of the gear mesh is nonlinear. The gear contact analysis includes a consideration of the calculated gear mesh misalignment and nonlinear tooth stiffness, as well as the detailed micro-geometric surface definition. The predicted contact position on the tooth flank will influence the gear mesh force. For example, if the contact is away from the center of the tooth, this will generate a turning moment on the gear, to which the supporting bearings will have to react. All of the gear meshing points, forces, load distributions, and boundary conditions are considered and analyzed [6]. To analyze the gear contact, the thin slice model can be used. This assumes that the gear (either helical or spur) is divided into a number of slices across the face width, each acting as a spur gear parallel to and independent from its neighboring slices. The gear contact can then be analyzed for these spur gear slices by approximating each as a spring of known stiffness and equating the sum of the loads with the total applied load [7].

The rolling element bearings added to the model include internal detail parameters such as the number, diameter, and length of the rolling elements; the diameter and curvature of the raceways; the internal clearance; and the roller profile, which allow the determination of the nonlinear stiffness for any load condition. The stiffness matrix for each bearing is obtained by linearizing the nonlinear behavior of the bearing at close to the operating condition and with the slope of the force versus deflection at the operating displacements of the bearing. The nonlinear stiffness matrix, linking the displacements and tilts of the geometric centers of the inner and outer raceways, includes the contacts of the rolling elements with the raceways, the nonlinear effects of the internal clearance, and the preload [6].

In order to include the stiffness properties and flexibility of nonuniform components such as the housing, ring gears, and planet carriers, these parts are imported as meshed finite element models (FEM). These finite element models are condensed to reduced stiffness matrices and coupled with the internal gearbox components through nodes of the bearings, shafts, and ring gears [8]. The shafts are also modeled as flexible beam elements.

Figure 2 shows that the PGS consists of the planet carrier FE model, nonlinear planet bearings, and planet gears. All of the planets are supported on planet pins through cylindrical roller bearings.

3 Design Load of Wind Turbine Gearbox

The design load of a WTG can be divided into two types: (i) an extreme load caused by the ultimate wind speed (e.g., wind turbulence) and (ii) a fatigue load caused by repeated loading during the service life. This is provided by a wind turbine system manufacturer [9]. The fatigue load, which is essential to evaluate the durability and life of the WTG, is composed of the load duration distribution (LDD) for the driving torque (M_{XN}) and non-torque loads. The non-torque loads include (F_{XN}, F_{YN}, F_{ZN}) and (M_{YN}, M_{ZN}), as shown in Fig. 3. These are the external loads, except for the torque, generated by fluctuating wind excitation when wind acts on the blades. Figure 3 shows the coordinate system for the design load of the WTG, where the origin is the hub center of the wind turbine system [9]. In this paper, the torque LDD provided by a system manufacturer is presented in Table 1, where the total duration of the torque LDD is 20 years to match the service life of the wind turbine system. The damage equivalent load (DEL) obtained from the LDDs for non-torque loads is presented in Table 2 and calculated using Eq. (1) [10]. The primary failure mode of the WTG is assumed to be the contact fatigue of the gears, and an n value of 6.61 is used for the contact fatigue [11].

$$P_{\text{equ}} = \sqrt[n]{\frac{\sum P_i^n t_i}{t}} \tag{1}$$

4 Face Load Factor and Mesh Load Factor

4.1 Face Load Factor for Contact Stress. The face load factor for contact stress, called the *load distribution factor,* takes into account the effect on the contact stress by the load distribution over the face width and is defined by Eq. (2) [11].

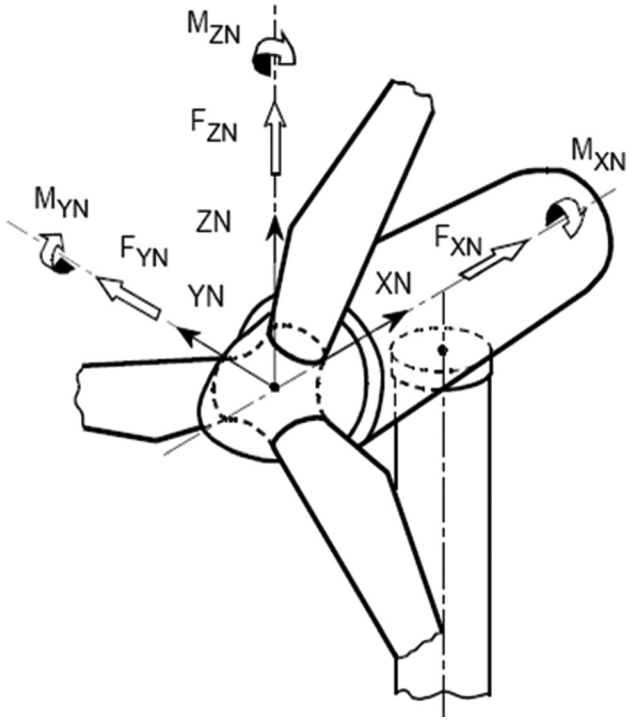

Fig. 3 Coordinate system of design load

Table 1 Torque LDD of wind turbine gearbox

Load case	Driving torque, kNm	Rotational speed, rpm	Duration, hours
1	180	0.2	22000
2	220	3.0	13000
3	310	8.5	11200
4	490	9.0	12100
5	640	11.0	23400
6	720	14.0	15000
7	940	14.5	14300
8	950	17.0	15000
9	1140	18.0	49000
10	1290	20.0	200
		Total duration	175200

Table 2 DEL of wind turbine gearbox

F_{XN}, kN	F_{YN}, kN	F_{ZN}, kN	M_{YN}, kNm	M_{ZN}, kNm
244	31	−400	730	595

$$K_{H\beta} = \frac{\text{maximum load per unit face width}}{\text{average load per unit face width}} = \frac{(F/b)_{\max}}{F_m/b} \quad (2)$$

An uneven load distribution along the face width can be caused by manufacturing errors and thermal distortions, as well as gear mesh misalignment in the plane of action, comprising a load-induced elastic deflection of the gears, flexibility of the housing and planet carriers, and deformation of the bearings.

4.2 Mesh Load Factor. The mesh load factor, called the *load sharing factor*, takes into account the uneven distribution of the load between meshes for multiple transmission paths and is defined by Eq. (3) [12].

$$K_\gamma = \frac{T_{\text{Branch}} N_{CP}}{T_{\text{Nom}}} \quad (3)$$

Load sharing among the planets of a PGS is influenced by many parameters such as the external load acting on gears, the bearing clearance, and the accuracy of manufacture.

5 Results of Analysis

The WTG models are simulated under operating speed and fatigue load conditions. The static deflections of the shafts, gears, and bearings are calculated while considering the flexibility of the housing, planet carriers, and ring gears. Also predicted are the effects on the planetary multiple meshes by the gear mesh misalignment, contact pattern, face load factor, and mesh load factor.

The analyses are performed using two models: the first model, called the *case I model*, considers only torque for the design load; the second model, called the *case II model*, considers non-torque loads as well as torque.

5.1 Analysis of System Deflections. Figure 4 shows a comparison of the system deflections for the case I model and case II model. It is found that the case II model generally has a larger deflection than the case I model, and there is a particular difference in the deflection of the low-speed shaft, where the fatigue load acts directly.

Figure 5 shows a comparison of the radial displacements of the low-speed shaft for the two models. It is confirmed that the low-speed shaft of the case II model has a higher radial displacement than that of the case I model, and it can be predicted that this leads a low-speed planet carrier connected with the low-speed shaft to have a relatively high radial displacement and restoring moment. Because of this phenomenon, the load distribution over the gears and the load sharing among the planets become uneven. This is because the radial displacement of the low-speed shaft is not zero under the case I model when considering the effect of the gravitational force during the analysis.

5.2 Analysis of Gear Mesh Misalignment. The gear mesh misalignment is calculated from the deflection of the shafts as

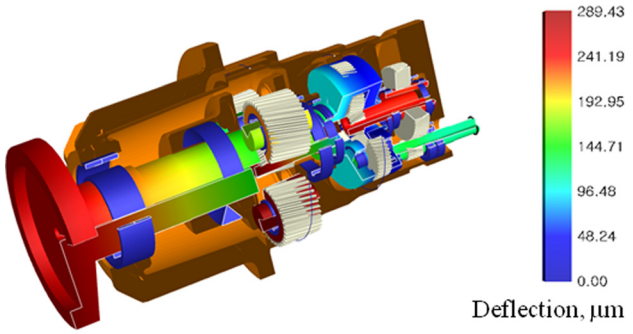

(a) System deflections of case I model

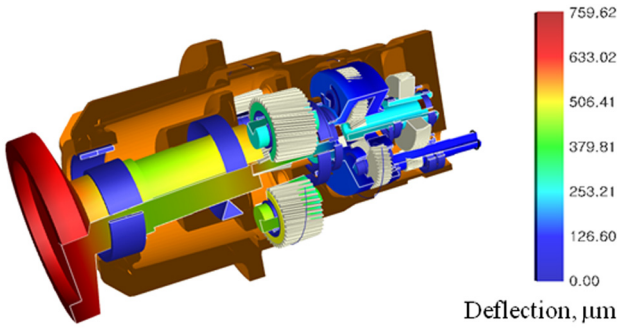

(b) System deflections of case II model

Fig. 4 Comparison of system deflections

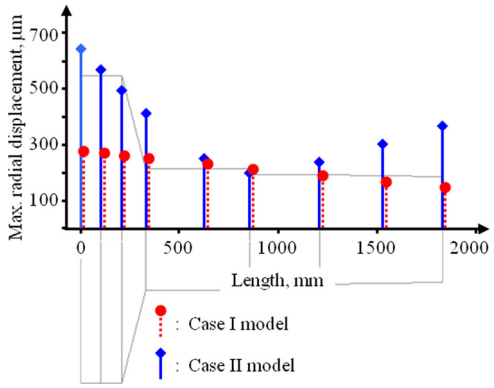

Fig. 5 Comparison of maximum radial displacements of low-speed shaft

well as the deformation and clearance of the bearings on which the gears are mounted, which is then converted to values along the line of action on the gear mesh. Accordingly, when this value is smaller, the load distribution of the gear mesh is more even. For convenience in the analysis, the signs are defined as shown in Fig. 6. This means that if the misalignment value is positive, the gear mesh occurs on the left side of the face width, and if the value is negative, the gear mesh occurs on the right side of the face width [13].

Figures 7(*a*) and 7(*b*) show $F_{\beta X}$ versus the carrier rotation angle for an LS PGS and HS PGS under the case II model, respectively. It is found that $F_{\beta X}$ varies periodically, depending on the carrier rotation angle, gear mesh (sun-planet, planet-ring), and position of a planet. This is because a large displacement and moment are generated at a low-speed planet carrier as a result of the non-torque loads acting on a low-speed shaft. The $F_{\beta X}$ value of the HS PGS also varies periodically as a result of the phenomenon mentioned above.

In the case of a sun-planet mesh of the LS PGS, it is found that $F_{\beta X}$ fluctuates periodically, so the gear mesh alternately occurs on the left and right sides of the face width. For a planet-ring mesh, it is also confirmed that $F_{\beta X}$ fluctuates periodically, so the gear mesh occurs on the left side of the face width. In the case of the

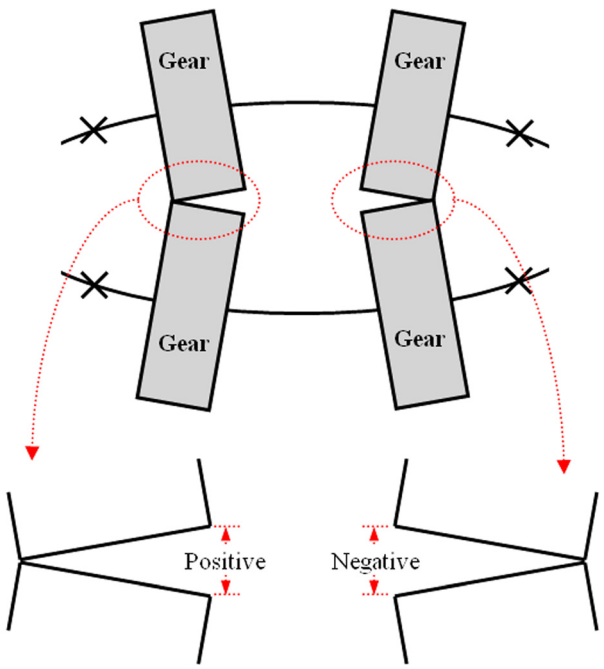

Fig. 6 Signs of gear mesh misalignment

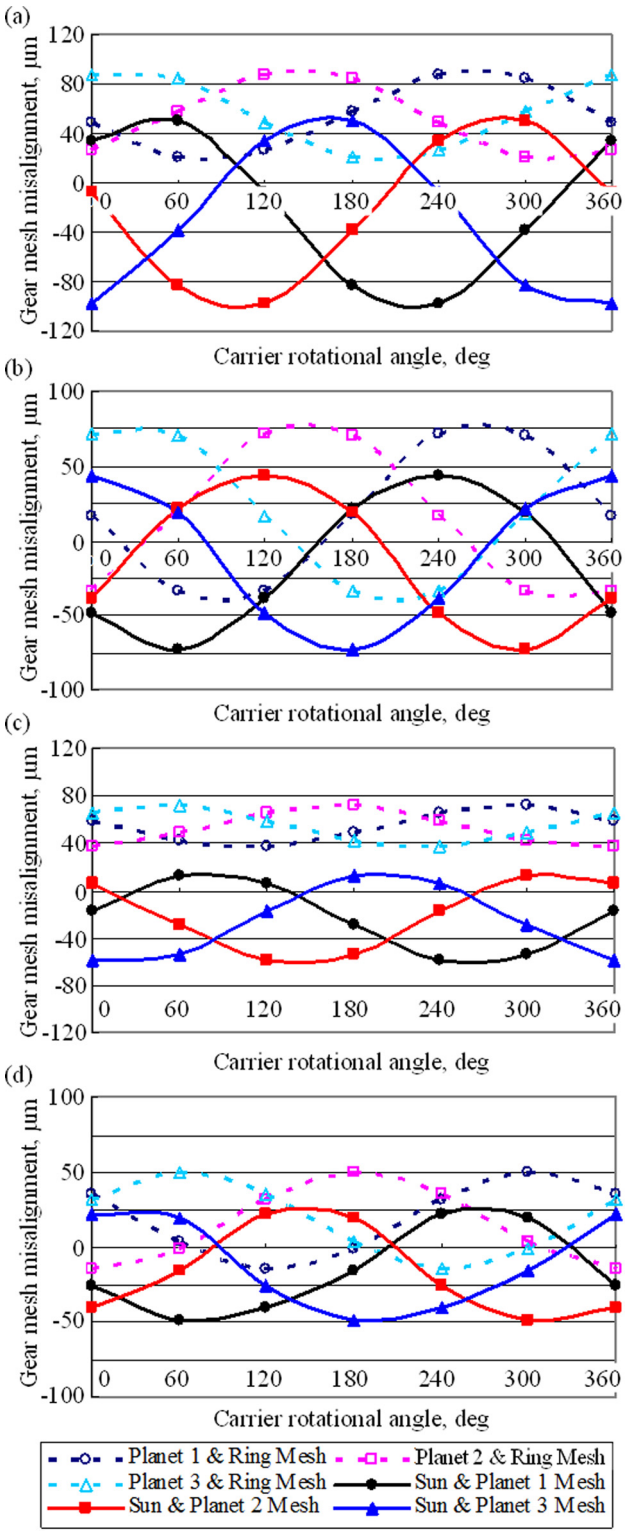

Fig. 7 Variation in gear mesh misalignment of (*a*) LS PGS, (*b*) HS PGS in case II model and (*c*) LS PGS, (*d*) HS PGS in case I model

HS PGS, it is found that $F_{\beta X}$ fluctuates periodically for a sun-planet mesh and planet-ring mesh, so the gear mesh alternately occurs on the left and right sides of the face width for both meshes.

Figures 7(*c*) and 7(*d*) indicate the $F_{\beta X}$ values for the case I model. It is again proved that $F_{\beta X}$ varies periodically, depending on the carrier rotation angle, gear mesh, and position of a planet,

like in Figs. 7(*a*) and 7(*b*). Although non-torque loads are not considered, periodic fluctuation is observed. This is the result of the effect of the gravitational force. A displacement of a planet carrier occurs because of the gravitational force, and this also induces fluctuation in the $F_{\beta X}$ values of the LS PGS and HS PGS.

As a result of the analysis, it can be confirmed that the gear mesh misalignments of the two PGSs are increased by considering the non-torque loads, and the gear mesh misalignment of the LS PGS (where the non-torque loads act directly on the carrier) is greater than that of the HS PGS.

5.3 Analysis of Load Distribution. The load distribution of a gear tooth flank can be evaluated using the face load factor, $K_{H\beta}$. The value of $K_{H\beta}$ can be calculated using a numerical formula (ISO 6336: method C) [11]. However, in this study, it is calculated with the contact pattern analysis method (ISO 6336: method B) [11] using commercial software [13].

Figures 8 and 9 show, respectively, the contact patterns of the sun-planet meshes and planet-ring meshes of the LS PGS under the case II model. The contact patterns of six meshes generated by three planets (three sun-planet meshes and three planet-ring meshes) are all different, and it is observed that for each mesh the load is distributed unevenly along the face width. The red parts of the figures indicate the high load acting on the gear tooth flank, and it is possible to understand the contact properties of the planetary multiple mesh through these figures.

From the mesh of the sun and planet 1 in Fig. 8(*a*), it is found that the gear mesh moves toward the left end of a tooth flank. Conversely, from the mesh of the sun and planet 2 in Fig. 8(*b*) or the sun and planet 3 in Fig. 8(*c*), it is found that the gear mesh moves toward the right end of a tooth flank, and the load distribution leans toward the right. This means that the gear contact pattern varies with the position of a planet. Moreover, as the gear mesh leans toward the left or right, the gear mesh area that transmits the load decreases. This may cause high contact stress, which will shorten the gear life. These phenomena also occur at the planet-ring mesh in Fig. 9. Although there is a difference in the contact load magnitude, a similar contact pattern is observed at the mesh in the case I model.

In the case of the model that considers non-torque loads, the gear mesh location on the tooth flank changes with respect to the planet position, so the magnitude and distribution of the load acting on the gear tooth flank also vary. This leads to a shorter gear life and causes gears to break early.

Table 3 lists the face load factors of the two models for the WTG and indicates the maximum $K_{H\beta}$ calculated when the misalignment is max or min depending on the carrier rotation angle.

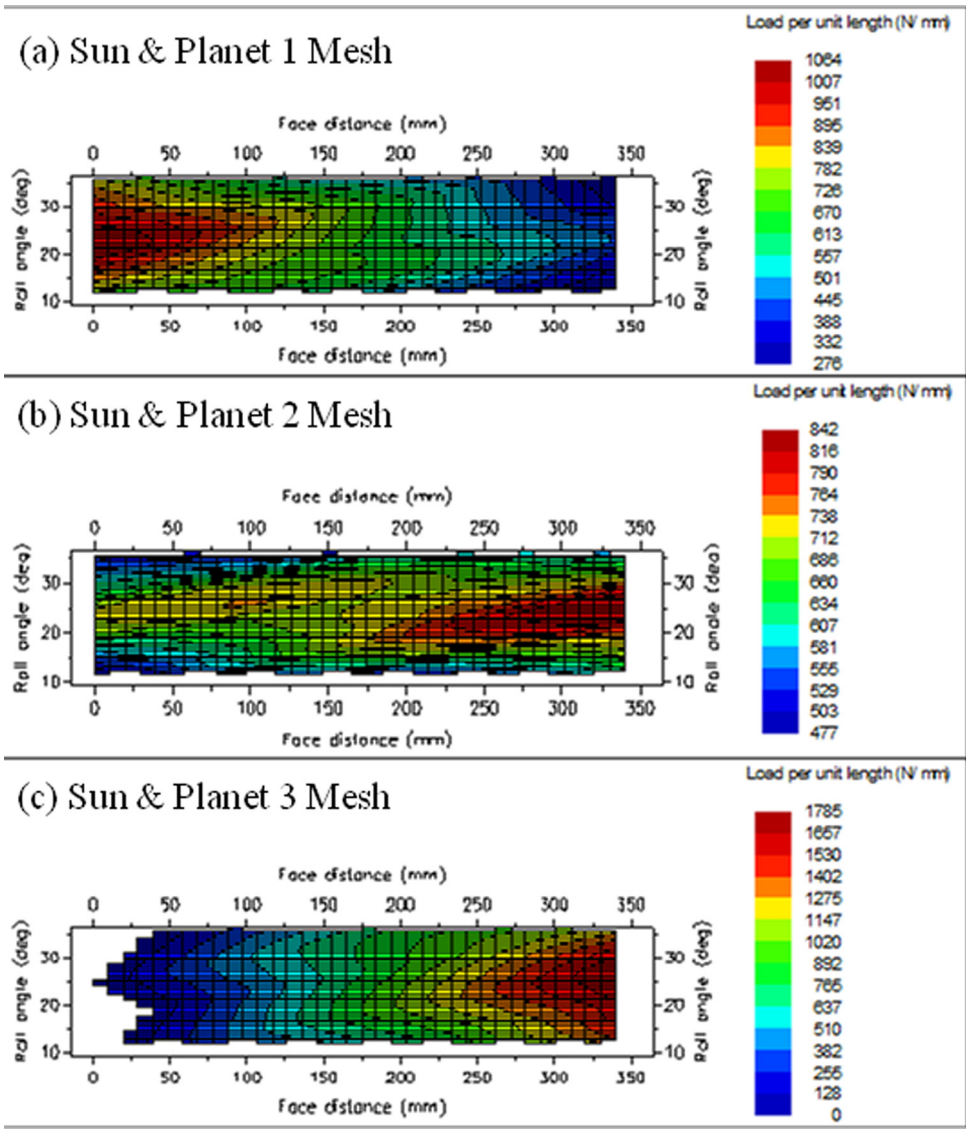

Fig. 8 Contact patterns of sun-planet meshes of LS PGS in case II model

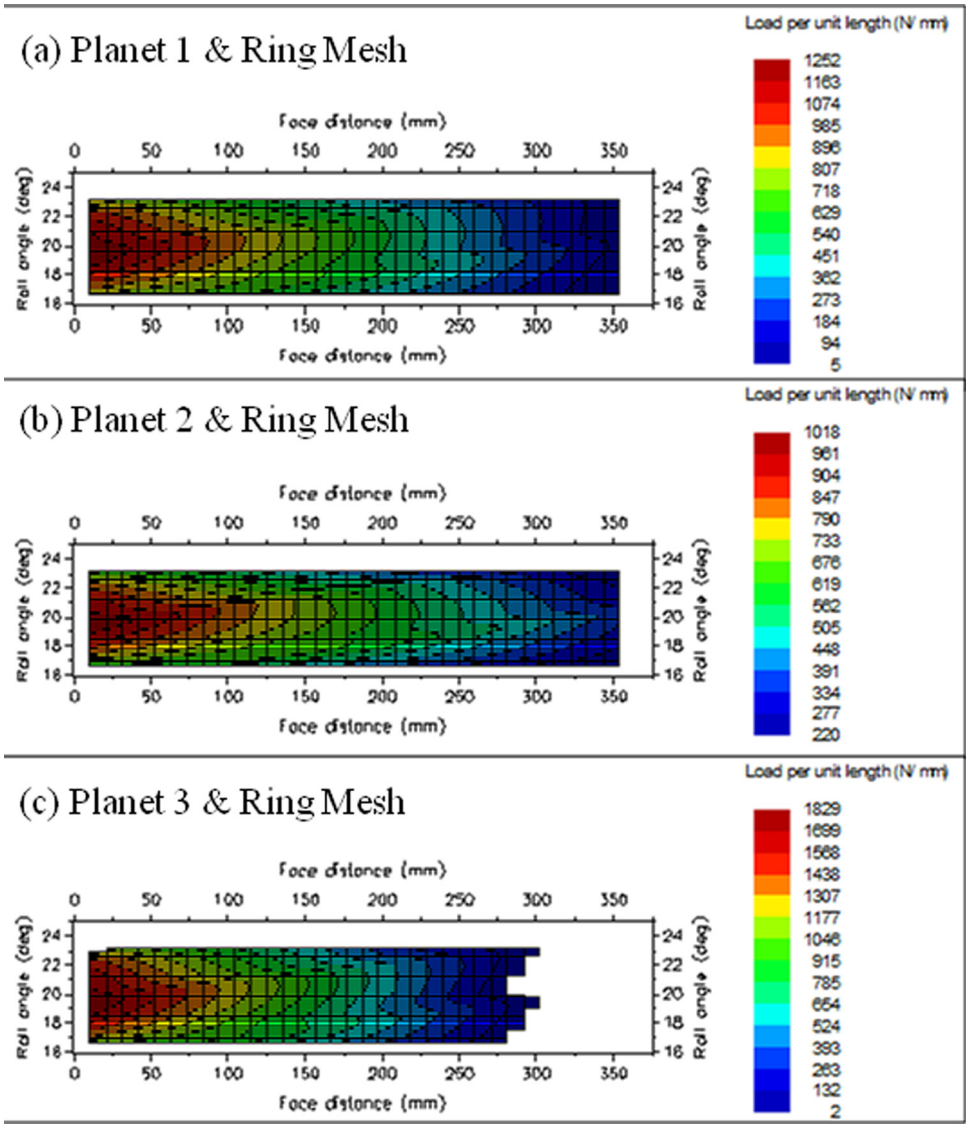

Fig. 9 Contact patterns of planet-ring meshes of LS PGS in case II model

Table 3 Comparison of face load factors

Case	PGS	Sun-planet mesh	Planet-ring mesh
I	LS	1.696	2.136
	HS	1.745	1.884
II	LS	2.082	2.397
	HS	1.836	2.766

Table 4 Comparison of gear safety factors

		Safety factor for contact stress		Safety factor for bending stress	
PGS	Gear	Case I	Case II	Case I	Case II
LS	Sun	1.132	0.998	2.239	1.782
	Planet	1.150	1.015	1.440	1.206
	Ring	2.218	2.067	1.509	1.303
HS	Sun	1.165	1.099	2.964	2.672
	Planet	1.257	1.130	2.103	1.680
	Ring	2.572	2.256	1.924	1.704

Table 4 lists the gear safety factors calculated using ISO 6336 method C [11]. The gear safety factor is inversely proportional to $K_{H\beta}$. Thus, if $K_{H\beta}$ is increased, the safety factor is decreased. For the case I model, which considers only torque for the design load, the gear safety factors are all greater than unity. However, for the case II model, which considers non-torque loads as well as torque, the safety factor for the contact stress of the sun gear of the LS PGS is less than unity.

In other words, it should be noted that the gear safety factor can vary, depending on which design load is used for the WTG. To guarantee the service life required by the WTG, it is very important to correctly define the design load for the gearbox.

5.4 Analysis of Load Sharing. The load sharing among the planets can be evaluated using the mesh load factor, K_γ. In this study, the value of K_γ is obtained from Eq. (2) after analyzing the torques acting on the planet pins by performing a computer-aided calculation [13]. The torques acting on the planet pins are predicted at seven discrete angular positions, which span a 360 deg rotation of the planet carriers under a quasi-static condition.

Figures 10(*a*) and 10(*b*) show the load sharing of the LS PGS and HS PGS, along with the torques acting on the planet pins as functions of the carrier rotation angle. The dotted lines represent the case I model. The solid lines represent the case II model. In Fig. 10, it is found that the torques acting on the three planet pins vary sinusoidally with respect to the rotation of the carriers.

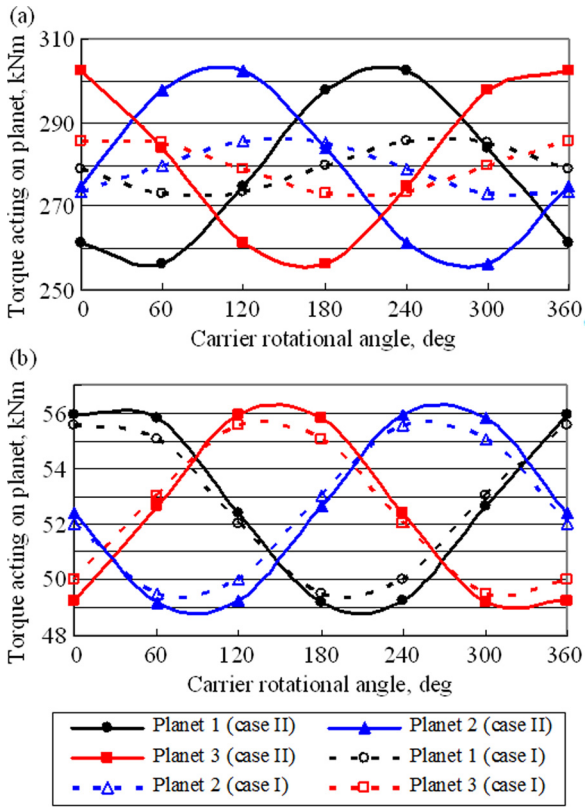

Fig. 10 Variation of torques acting on planet pins of (*a*) LS PGS and (*b*) HS PGS in case I and II models

Table 5 Comparison of mesh load factors

Case	PGS	K_γ
I	LS	1.026
	HS	1.065
II	LS	1.092
	HS	1.074

Comparing the results of the case I model and case II model, the relative torque fluctuation of the case II model is greater than that of the case I model, which means the relative fluctuation in the torque acting on a planet pin increases when non-torque loads are considered. Moreover, the torque fluctuation of the LS PGS is greater than that of the HS PGS, which means the load sharing of the LS PGS is more uneven than that of the HS PGS.

Table 5 lists the mesh load factors of the PGS for each of the two models. It can be confirmed that the mesh load factors of the case II model are increased by considering the non-torque loads, and the K_γ of the LS PGS (where the non-torque loads act directly on the carrier) is greater than that of the HS PGS in the case II model. The value of K_γ is inversely proportional to the gear safety factor, like $K_{H\beta}$. Thus, K_γ should be reduced in order to improve the gear safety factor.

6 Conclusions

In this study, a state-of-the-art nonlinear system model was developed to analyze the planetary gearset for a WTG, and the developed model was applied to investigate how the external loads caused by wind fluctuation influence both the load distribution on the gear tooth flank and the planet load sharing. This model considers the gear mesh stiffness and bearing stiffness as nonlinearities and the housing, planet carriers, and ring gears as deformable bodies. Two models for different design loads were employed to quantify how the external loads acting on the input shaft of the WTG affect the load distribution of the gears and the load sharing among the planets under the quasi-static conditions. One model considered only the torque for the design load, whereas the other model also considered the non-torque loads. A comparative analysis was performed for the two models. Based on the results presented, the following conclusions can be drawn:

(1) In order to accurately predict the loads acting on the gears and the gear mesh misalignment, it is very important to model and analyze the whole WTG simultaneously through a system level analysis. This is because the gear mesh misalignment, which is the basis for estimating the load distribution and load sharing, depends on the deflection of the shafts and the deformation of the bearings, as well as the flexibility of the housing, planet carriers, and ring gears. Therefore, it may not be easy to predict the distribution and sharing of loads exactly using a component level analysis. By taking advantage of modeling the gearbox system as a whole, the model can predict the system deflections more accurately. This makes it possible to determine the effects of misalignment on the gear and bearing durability.

(2) For two models with different design loads, the results for the gear mesh misalignment, contact pattern, load distribution, and load sharing were respectively different, which led to different gear safety factors. If the gears are assumed to be safe when the gear safety factor is greater than unity, the gears for the case I model turned out to be safe, while those for the case II model turned out to be unsafe. In other words, the gear safety factor can be varied by changing the design load. Therefore, the design load can also affect the gear rating.

(3) The results presented indicate that it is appropriate to consider the non-torque loads caused by wind fluctuation; in addition to the torque, as the design load for a WTG, and that this is very important to accurately determine a design load that guarantees the service life of the WTG.

Nomenclature

b = gear face width
F = load on arbitrary position of tooth flank
F_m = mean load at the reference circle
F_{XN} = thrust force in direction of rotor axis
F_{YN} = side force at rotor
F_{ZN} = weight force at rotor
$F_{\beta X}$ = gear mesh misalignment
$K_{H\beta}$ = face load factor for contact stress
K_γ = mesh load factor
M_{XN} = driving torque at rotor
M_{YN} = tilting moment at rotor
M_{ZN} = yaw moment at rotor
N_{CP} = number of planets
n = slope of the Woehler-damage line
P_{equ} = damage equivalent load for non-torque loads
P_i = load level for load case i
T_{Branch} = torque in branch with heaviest load
T_{Nom} = total nominal torque
t = accumulated time
t_i = duration for load case i

References

[1] Spinato, F., Tavner, P., Bussel, G., and Koutoulakos, E., 2009, "Reliability of Wind Turbine Subassemblies," IET Renewable Power Generation, **3**(4), pp. 1–15.

[2] Lee, G. H., Park, Y. J., Kim, J. K., Yim, J. G., Nam, Y. Y., and Chong, T. H., 2009, "An Optimal Design for MW-Class Wind Turbine Gearboxes Based on Their Structural Characteristics," Proceedings of the 8th World Wind Energy Conference and Exhibition, pp. 101–109.

[3] Bodas, A., and Kahraman, A., 2004, "Influence of Carrier and Gear Manufacturing Errors on the Static Load Sharing Behavior of Planetary Gear Sets," JSME Int. J., Ser. C, **47**, pp. 908–915.
[4] Singh, A., 2005, "Application of a System Level Model to Study the Planetary Load Sharing Behavior," ASME J. Mech. Design., **127**, pp. 469–476.
[5] Kahraman, A., and Vijayakar, S., 2001, "Effect of Internal Gear Flexibility on the Quasi-Static Behavior of a Planetary Gear Set," ASME J. Mech. Design., **123**, pp. 408–415.
[6] Pears, J., Smith, A., Platten, M., Willson, B., Cheng, Y., and Felice, M., 2007, "Predicting Variation in the NVH Characteristics of an Automatic Transmission Using a Detailed Parametric Modeling Approach," SAE 2007 Noise and Vibration Conference and Exhibition, SAE Paper No. 2007-01-2234.
[7] Pears, J., Curtis, S., Poon, A., Smith, A., Poon, D., and Palmer, D., 2005, "Investigation of Methods to Predict Parallel and Epicyclic Gear Transmission Error," 2005 SAE World Congress, SAE Paper No. 2005-01-1818.
[8] Kamaya, F., Eccles, M., and Pears, J., 2008, "A Rapid Method for the Investigation of System-Wide Parameter Variation Effects on Epicyclic Gear Whine," Trans. Soc. Automot. Eng. Japan **39**(6), pp. 647–652.
[9] Wind Energy Committee, *Guideline for the Certification of Wind Turbines* (Germanischer Lloyd, WindEnergie GmbH, Hamburg, Germany, 2003).
[10] Niederstucke, B., Anders, A., Dalhoff, P., and Grzybowski, R., *Load Data Analysis for Wind Turbine Gearboxes* (Germanischer Lloyd WindEnergie GmbH, Hamburg, Germany, 2003).
[11] International Organization for Standardization (ISO), 2007, "Calculation of Load Capacity of Spur and Helical Gears," Paper No. ISO 6336-(1:6).
[12] American Gear Manufacturers Association (AGMA), 2006, "Design Manual for Enclosed Epicyclic Gear Drives," Paper No. ANSI/AGMA 6123-B06.
[13] Romax Technology Ltd., *RomaxDesigner Software Handbook* (Romax Technology Ltd., Nottingham, UK, 2006).